Optica Applicata, Vol. LIII, No. 4, 2023
DOI: 10.37190/oa230402

Finite difference time domain method of light propagation through inhomogeneous media

M. Milosevic, N. Stevanovic*, V.M. Markovic, Z. Cimbaljevic

Faculty of Science, University of Kragujevac,
R. Domanovic 12, 34000 Kragujevac, Serbia

*Corresponding author: nstevanovic@kg.ac.rs

Propagation of arbitrarily polarized light through inhomogeneous media is modeled in this paper. The model can include parameters of the media such as relative dielectric constant, relative magnetic constant and electric conductivity. The orientation of the electric field strength of the light source could be defined arbitrarily, and in this paper two polarization modes are considered: transverse electric (TE) mode and transverse magnetic (TM) mode. The electric field vector could change its orientation in dependence on the characteristics of the media. The model developed in this paper is based on the finite difference time domain (FDTD) method and Maxwell's equations. A two-dimensional formulation of FDTD is applied in this computing. Several cases were considered, and the results obtained in this paper agree with the literature. The model shown in this paper does not require much time for computer processing and can be easily applied for specific cases of media, source, and light.

Keywords: FDTD method, optics, light propagation.

1. Introduction

A great number of papers are devoted to the problem of the propagation of light through arbitrary media [1-5]. The distribution of light intensity that passes through a slit or obstacle was considered in [6-14], where Fraunhofer or Fresnel diffraction were considered. The aim of the referenced papers was to correlate the shape and dimensions of slit/obstacle and diffraction pattern properties. These papers deal with regular 2D surfaces such as rectangle and circle as obstacles through light passes. There are a few papers devoted to the diffraction of light on a 3D object [15-19]. The most common method for simulation of light propagation is Huygens–Fresnel (HF) principle. Using this principle, diffraction patterns created from the diffraction of light on the arbitrary surface, which bounds two media of arbitrary refractive index, can be reconstructed. The diffraction pattern in the case of Fraunhofer diffraction is observed on the distant screen. Similar method was presented in [20], for Fresnel diffraction on a plane

screen, from a surface extended source. The model in [20] was based on FFT (fast Fourier transform) and could be applied for Fresnel diffraction where the distance to the screen is much larger than the surface dimensions.

The models of light transport given in papers [6-19] have several assumptions, on which they are built.

The first assumption is that the incident wavefront is plane [6-14]. The electric field vector is parallel to the considered surface between the two media and does not change its orientation during light propagation. These changes in orientation were not considered even if point-like sources were considered, where the electric field vector cannot lie in the plane of the 2D boundary surface. For large distances of the point source to the obstacle or boundary surface, compared to the size of the obstacle, this could be a reasonably good approximation. Propagation of light through 3D surfaces was treated in [15,16] where changing of orientation electric field vector was also not considered. The dependence of light intensity on the phase shift of propagated light was calculated. Improvement of the HF model in [15,16] was done in [19], where a minimal system that emits light is taken to be an electric dipole. Each surface segment was treated as an electric dipole. In this approach, according to appropriate laws, the electric field changes orientation at the boundary.

The second assumption of light transport is that considered media is homogenous and refractive index is constant and does not depend on the coordinates [6-19]. The third assumption is that the conductivity of transparent media is equal to zero and cannot be considered in above referenced models.

One of the successful methods for the propagation of light is the application of the energy flow equation through the medium. Such a method is successfully used for investigation of the light propagation through optical fibers [20-22], elements of communication, optical instruments, *etc*. However, for elements with inhomogeneous and conductive media this method was not successful.

In the present paper, the model for the light propagation through arbitrary surface and inhomogeneous media was developed. This model is based on numerical solutions of time-dependent Maxwell's equations, using finite difference time domain – FDTD methods [24]. This model enables the propagation of electromagnetic waves at arbitrary frequencies (visible light, RF, UV, IR radiation) and arbitrary media. The method was used to simulate the propagation of light through the arbitrary surface between two media (plane, spherical, conical) and through inhomogeneous media, where the refractive index is changing gradually. An additional advantage of this model is that light can be propagated through conductive and more complex media, such as biological cells and tissues.

2. Methodology

2.1. Finite difference time domain (FDTD) method

FDTD method [24-27] for numerical simulation of propagation of electromagnetic waves is based on Maxwell's equations in differential form

$$-\sigma_{\mathrm{m}}\mathbf{H} - \mu\frac{\partial \mathbf{H}}{\partial t} = \nabla \times \mathbf{E} \tag{1}$$

$$\sigma\mathbf{E} + \varepsilon\frac{\partial \mathbf{E}}{\partial t} = \nabla \times \mathbf{H} \tag{2}$$

Here, **E** is the vector of the electric field, **H** is the vector of the magnetic field, μ and ε are magnetic and electric permittivity, respectively, while σ is electric conductivity of media. The magnetic conductivity σ_{m} is taken to be zero in this paper, as the characteristics of transparent material. Obstacles are inserted in the media and are presented in two dimensions (2D). Obstacles can be, for example, a plane in the Cartesian coordinate system, a circle, the cross-section of a cone and a plane. There are two polarizations that can be taken into account, regarding the orientation of the vector of the electric or magnetic field. This corresponds to the TE wave (electric field vector normal to *xOy* plane) and TM wave (magnetic field vector normal on *xOy* plane), as it is presented in Fig. 1. In both cases, the analysis is done using the sinusoidal incident wave.

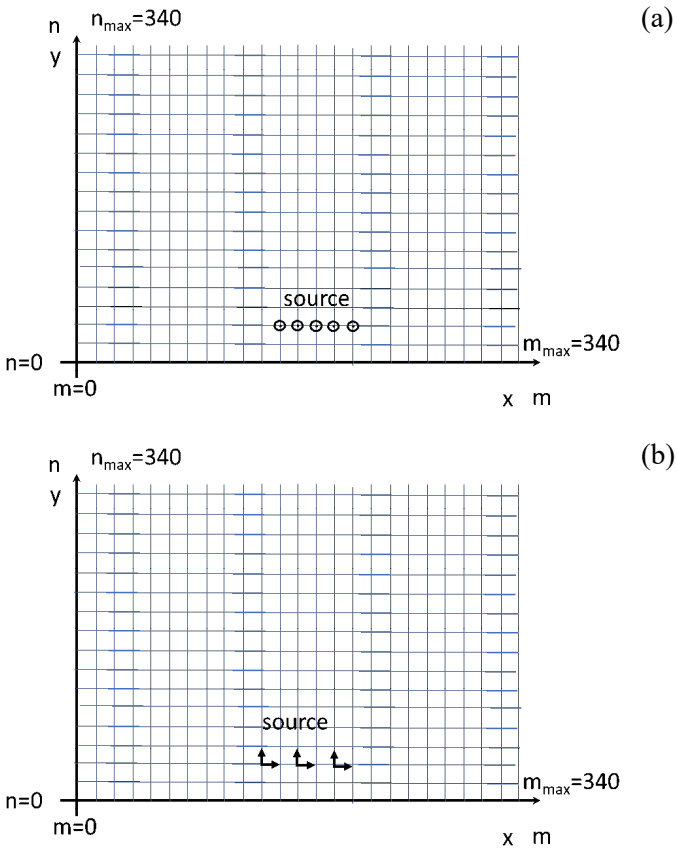

Fig. 1. Grid in the *xOy* plane and source for (a) TE mode with E_z component of electric field, and (b) TM mode with E_x and E_y components of electric field.

2.1.1. TE mode

The TE mode sets up the electric field transverse to wave propagation, directed toward the z-axis. In this mode three components of EM field are considered, one component of electric and two components of magnetic field (H_x, H_y, E_z). Other components of the EM field are equal to zero. The set of equations (1) and (2) in scalar form becomes

$$-\mu \frac{\partial H_x}{\partial t} = \frac{\partial E_z}{\partial y} \tag{3}$$

$$\mu \frac{\partial H_y}{\partial t} = \frac{\partial E_z}{\partial x} \tag{4}$$

$$\sigma E_z + \varepsilon \frac{\partial E_z}{\partial t} = \frac{\partial H_y}{\partial x} - \frac{\partial H_x}{\partial y} \tag{5}$$

The first and second equations give the derivation of the magnetic field over time, being proportional to the derivation of the electric field over spatial coordinates. Conversely, the third equation gives the derivation of the electric field over time, being proportional to the derivation of the magnetic field over spatial coordinates. These equations can be transformed in finite difference notation introducing a time and space grid. In discretized form Eqs. (3-5) take the form [24]

$$H_x^{q+1/2}[m, n] = H_x^{q-1/2}[m, n] - \frac{\Delta t}{\mu \Delta y}\left(E_z^q[m, n+1] - E_z^q[m, n]\right) \tag{6a}$$

$$H_y^{q+1/2}[m, n] = H_y^{q-1/2}[m, n] + \frac{\Delta t}{\mu \Delta x}\left(E_z^q[m+1, n] - E_z^q[m, n]\right) \tag{6b}$$

$$\begin{aligned} E_z^{q+1}[m, n] = {} & \left(1 - \frac{\sigma \Delta t}{2\varepsilon}\right)\left(1 + \frac{\sigma \Delta t}{2\varepsilon}\right)^{-1} E_z^q[m, n] \\ & + \left(1 + \frac{\sigma \Delta t}{2\varepsilon}\right)^{-1} \frac{\Delta t}{\varepsilon \Delta x}\left(H_y^{q+1/2}[m, n] - H_y^{q+1/2}[m-1, n]\right) \\ & - \left(1 + \frac{\sigma \Delta t}{2\varepsilon}\right)^{-1} \frac{\Delta t}{\varepsilon \Delta y}\left(H_x^{q+1/2}[m, n] - H_x^{q+1/2}[m, n-1]\right) \end{aligned} \tag{6c}$$

where spatial steps are between successive points in x and y coordinates and Δt is the time step. Indexes m and n correspond to spatial and q to time coordinates. In this paper, we introduced a square grid, where $\Delta y = \Delta x = \Delta$.

2.1.2. TM mode

The TM mode sets up the magnetic field transverse to wave propagation, and is directed towards the z-axis (H_z). The electric field has two components (E_x, E_y). For TM mode, the sets of equations (1) and (2) in the scalar form are

$$-\mu \frac{\partial H_z}{\partial t} = -\frac{\partial E_x}{\partial y} + \frac{\partial E_y}{\partial x} \tag{7}$$

$$\sigma E_x + \varepsilon \frac{\partial E_x}{\partial t} = \frac{\partial H_z}{\partial y} \tag{8}$$

$$\sigma E_y + \varepsilon \frac{\partial E_y}{\partial t} = -\frac{\partial H_z}{\partial x} \tag{9}$$

Applying the finite difference method, these equations can be written in the following form

$$H_z^{q+1/2}[m, n] = H_z^{q-1/2}[m, n] + \frac{\Delta t}{\mu}\left(\frac{E_x^q[m, n+1] - E_x^q[m, n]}{\Delta y} - \frac{E_y^q[m+1, n] - E_y^q[m, n]}{\Delta x}\right) \tag{10a}$$

$$E_x^{q+1}[m, n] = \left(1 - \frac{\sigma \Delta t}{2\varepsilon}\right)\left(1 + \frac{\sigma \Delta t}{2\varepsilon}\right)^{-1} E_x^q[m, n] + \Delta t\left(1 + \frac{\sigma \Delta t}{2\varepsilon}\right)^{-1} \varepsilon^{-1} \frac{H_z^q[m, n] - H_z^q[m, n-1]}{\Delta y} \tag{10b}$$

$$E_y^{q+1}[m, n] = \left(1 - \frac{\sigma \Delta t}{2\varepsilon}\right)\left(1 + \frac{\sigma \Delta t}{2\varepsilon}\right)^{-1} E_y^q[m, n] - \Delta t\left(1 + \frac{\sigma \Delta t}{2\varepsilon}\right)^{-1} \varepsilon^{-1} \frac{H_z^q[m, n] - H_z^q[m-1, n]}{\Delta x} \tag{10c}$$

By discretizing the equations, coordinates x and y are translated to the discrete coordinates m and n, respectively. In this way, the grid of the xOy plane is formed in the Cartesian coordinate system (Fig. 1). For each point of the grid, defined by the points with coordinates (m, n), the values of the medium characteristics are defined: electric conductivity $\sigma[m, n]$, electric permittivity $\varepsilon[m, n]$ and magnetic permeability $\mu[m, n]$.

If these values are equal at each point, then the medium is homogeneous, otherwise it is inhomogeneous. At the initial moment, $q = 0$ values of electric and magnetic field strength are equal to zero at all points of the grid, except at the point of source. In the next time step, the values of fields are calculated using the values of fields in the previous time step, for each point (m, n) of the grid. In Fig. 1 the sample of sources with TE and TM modes are shown. For TE mode, the vector of electric field strength E_z is orthogonal to the xOy plane, while for TM mode electric field vector is tangential to xOy plane and has two components: one orientated along the x-axis, E_x and another orientated along the y-axis, E_y.

2.2. Simulation of light propagation

To simulate light propagation through inhomogeneous media, software named Light-Propagation was developed. 2D matrix was formed with dimensions of $m \times n$ number of elements as presented in Fig. 1. Numbers m and n can be arbitrarily taken. In further simulations m and n have been equal to 340. The spatial step Δ depends on the wavelength and literature criteria is tenth part of the value of λ [22,23]. In this paper, the wavelength is set to $\lambda = 633$ nm, defining $\Delta = 63.3$ nm. To fulfill the stability of the calculation, the time step must satisfy condition $\Delta t \leq \Delta/(2c_0)$, where c_0 is the light velocity in a vacuum. Otherwise, solutions can diverge. In this work $\Delta t = 1.055 \times 10^{-16}$ s. The number of time steps in simulation is 1500 which corresponds to the total time of light propagation as equal to $1500\Delta t$. The time of the one light oscillation is $T = \lambda/c_0 = 2.11 \times 10^{-15}$ s. The number of time steps during the one period of oscillation is $S = T/\Delta t = 20$.

For each node (m, n) of the grid, parameters $\sigma[m, n]$, $\varepsilon[m, n]$ and $\mu[m, n]$ are set. If two homogenous media are treated, which are divided with the surface $F(x, y) = F_{mn}(m, n) = 0$, then the grid elements have one value on the one side of the surface, and the different on the other side of the boundary surface. In condensed form, the set of Eqs. (6) and (10) could be written as

$$H_x[m, n, q+1] = C_{hxh}[m, n] H_x[m, n, q] - C_{hxe}[m, n]\Big(E_z[m, n+1, q] - E_z[m, n, q]\Big) \tag{11a}$$

$$H_y[m, n, q+1] = C_{hyh}[m, n] H_y[m, n, q] + C_{hye}[m, n]\Big(E_z[m+1, n, q] - E_z[m, n, q]\Big) \tag{11b}$$

$$E_z[m, n, q+1] = C_{eze}[m, n] E_z[m, n, q] + C_{ezh}[m, n]\Big[\Big(H_y[m, n, q] - H_y[m-1, n, q]\Big) - \Big(H_x[m, n, q] - H_x[m, n-1, q]\Big)\Big] \tag{11c}$$

$$H_z[m, n, q+1] = C_{hzh}[m, n]H_z[m, n, q] + C_{hxe}[m, n]\left[\left(E_x[m, n+1, q] - E_x[m, n, q]\right) - \left(E_y[m+1, n, q] - E_y[m, n, q]\right)\right] \tag{12a}$$

$$E_x[m, n, q+1] = C_{exe}[m, n]E_x[m, n, q] + C_{exh}[m, n]\left(H_z[m, n, q] - H_z[m, n-1, q]\right) \tag{12b}$$

$$E_y[m, n, q+1] = C_{eye}[m, n]E_y[m, n, q] + C_{eyh}[m, n]\left(H_z[m, n, q] - H_z[m-1, n, q]\right) \tag{12c}$$

where C are matrix elements which depend on the media parameters.

Subscripts of coefficients were introduced to describe the creation of the field. The first index shows which field is being formed, the second index shows the component of that field, and the third index presents the source of created field. For example, subscript *eyh* means that the *y* component of the electric field is formed due to the magnetic field.

The value of magnetic or electric field strength in the node (m, n) in time step $q + 1$ depends on values of the field in that and adjacent elements in the previous step time.

When components of the electric and magnetic field in some moments of time are determined, the intensity of the light wave can be calculated as a module of the mean value of the Poynting vector

$$I = |\langle \mathbf{P} \rangle| = |\langle \mathbf{E} \times \mathbf{H} \rangle| \tag{13}$$

where $\langle \mathbf{P} \rangle$ is the mean value of the Poynting vector over time for one period of oscillation

$$\langle \mathbf{P} \rangle = \frac{1}{T}\int_0^T (\mathbf{E} \times \mathbf{H})\,\mathrm{d}t \tag{14}$$

3. Results and discussion

The model presented in this work can be applied for simulation of light propagation through an arbitrary surface. To apply the model, a plane coordinate system must be chosen, with discretized coordinates *m* and *n*. The authors chose a grid with 340 × 340 nodes, which is appropriate for the calculations presented below in the text. For each node of the grid, the parameters of the media must be known. The electric field strength of the source for TE mode is set as

$$E_z[m, n, t] = E_0 \cos(\omega t) \tag{15}$$

and for TM mode

$$E_x[m, n, t] = E_0 \cos(\omega t) \text{ and } E_y[m, n, t] = E_0 \cos(\omega t) \tag{16}$$

where $\omega = 2\pi/T$ and $E_0 = 1$ V/m is the electric field amplitude. The values of m and n are chosen depending on the considered case, which will be explained further in the text.

3.1. Light propagation in two media bounded by a plane surface

In this part the propagation of light in two homogenous media bounded with the plane was considered. Equation of plane is set to be (it is fully arbitrary)

$$F(m, n) = n - (m - 170)\tan\alpha - 170 = 0 \tag{17}$$

This plane surface goes through the center of the grid ($m_c = 170$, $n_c = 170$) and forms angle α with the m-axis. If $\alpha = 0$, this case corresponds to the plane which is parallel to m-axis. If $\alpha > 0$, then the plane has a slope with α in respect to m-axis (Fig. 2).

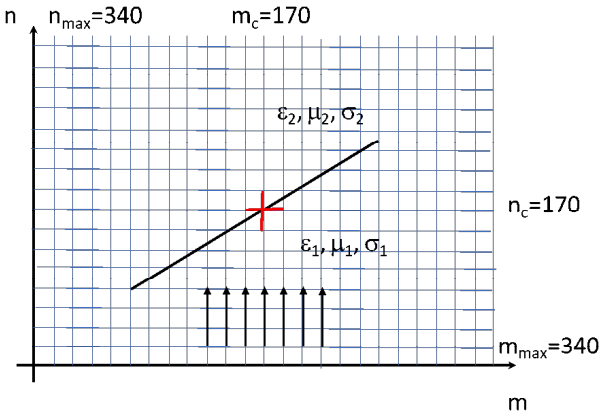

Fig. 2. Media grid with considered plane through which light propagates.

The intensity of light propagation through two media bounded by a plane was presented in Fig. 3. Parameters of media have following values $\sigma[m, n] = 0$ and $\mu[m, n] = \mu_0$ for each m and n. Relative dielectric constant $\varepsilon[m, n] = 1$ for n larger than defined by Eq. (17), and $\varepsilon[m, n] = 2.25$ for other. The intensity of light of TE mode propagating from media with a larger optical density to media with a lower optical density was presented in Fig. 3(a). The angle of the plane slope with respect to m-axis is $\alpha = \pi/4$ rad. It could be seen that light directed from bottom has total reflection, as it could be predicted by geometrical optics. The surface and angles of incident and reflected light were presented in the figure. The angle of the surface with respect to the m-axis is $\pi/4$ rad, the angle of incident light and normal to the surface is $\pi/4$ rad as well as the angle of reflected light.

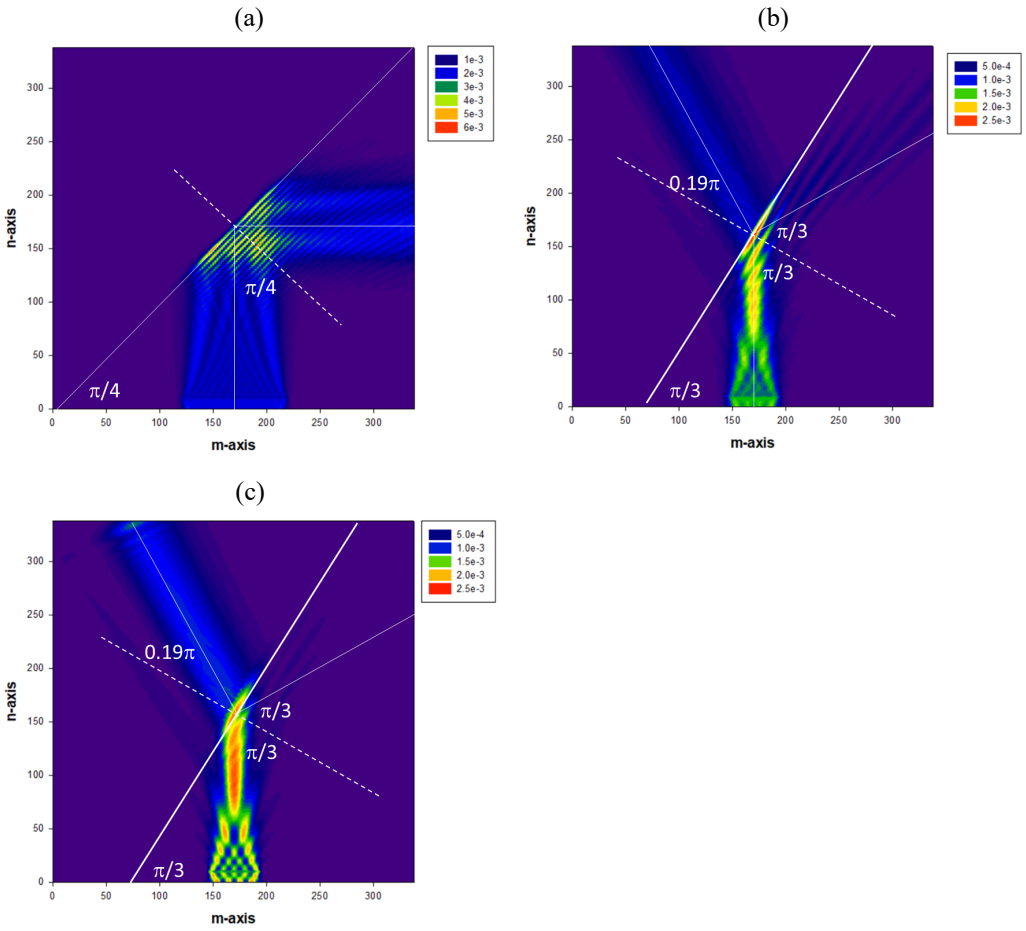

Fig. 3. Propagation of light through a plane. (a) Light intensity of TE mode that propagates from the media with larger to the lower optical density, where $\alpha = \pi/4$ rad. (b) Light intensity of TE mode that propagates from the media with lower to the larger optical density, where $\alpha = \pi/3$ rad. (c) Light intensity of TM mode that propagates from the media with lower to the larger optical density, where $\alpha = \pi/3$ rad.

Figure 3(b) presents the light intensity of the light with a case where $\varepsilon[m, n] = 1$ is constant for n smaller than defined by Eq. (17), and $\varepsilon[m, n] = 2.25$ for other values of n. The angle of the plane is $\alpha = \pi/3$ rad. It could be clearly seen that there are transmitted and reflected parts of the light. The angle of transmitted light in respect to the normal of the surface is 0.19π rad and the angle between the surface and m-axis is $\pi/3$ rad. The mode of light considered in this case is TE (s-polarization).

Fresnel coefficients for reflected and transmitted light respectively are [27]

$$R_s = \left(\frac{n_i \cos\theta_i - n_t \cos\theta_t}{n_i \cos\theta_i + n_t \cos\theta_t} \right)^2 = 0.17 \tag{18a}$$

$$T_{\mathrm{s}} = \left(\frac{2n_{\mathrm{i}}\cos\theta_{\mathrm{i}}}{n_{\mathrm{i}}\cos\theta_{\mathrm{i}} + n_{\mathrm{t}}\cos\theta_{\mathrm{t}}} \right)^2 = 0.33 \tag{18b}$$

This result was obtained by the FDTD method where the intensity of transmitted light is about two times larger than reflected as could be seen in Fig. 3(b).

In Fig. 3(c) intensity of light with TM mode (*p*-polarization) was presented. Here it was taken that the electric field of the source has a projection $E_x[m, n, t] = E_0\cos(\omega t)$ while $E_y = 0$. According to Fresnel formulas, the *p*-polarized, coefficients of reflected and transmitted light are

$$R_{\mathrm{p}} = \left(\frac{n_{\mathrm{i}}\cos\theta_{\mathrm{t}} - n_{\mathrm{t}}\cos\theta_{\mathrm{i}}}{n_{\mathrm{i}}\cos\theta_{\mathrm{t}} + n_{\mathrm{t}}\cos\theta_{\mathrm{i}}} \right)^2 = 0.001 \tag{19a}$$

$$T_{\mathrm{p}} = \left(\frac{2n_{\mathrm{i}}\cos\theta_{\mathrm{i}}}{n_{\mathrm{i}}\cos\theta_{\mathrm{t}} + n_{\mathrm{t}}\cos\theta_{\mathrm{i}}} \right)^2 = 0.4 \tag{19b}$$

The reflected wave has weaker intensity, as obtained in this paper (see Fig. 3(c)).

3.2. Light propagation through the spherical surface

In this part, the light propagation was observed through the spherical surface, with a radius $R = 50\Delta$. In discretized grid, the center of sphere is in coordinates (170, 170), and its equation is

$$F(m, n) = (m - 170)^2 + (n - 170)^2 = 50^2 \tag{20}$$

The relative electric constant of the medium outside of the sphere is $\varepsilon_{r_1} = 1$ and in the sphere is $\varepsilon_{r_2} = 2.25$. It corresponds to the case of refractive index in sphere 1.5 and 1 outside sphere. The wavelength of light is $\lambda = 633$ nm.

Figure 4(a) shows the strength of the electric field of the light wave after $1500\,\Delta t$ time. It can be seen in the picture that the refraction of the wavefront occurs at the boundary surface of the two media. If it passes from an optically less dense to an optically denser medium, the highest value of the electric field is at a point on the surface and axis of the sphere. Constructive interference of the incident wavefront occurs at that point. At that point the intensity of light has the highest value (Fig. 4(b)), and it represents the focal point of that system (convex converging lens), which can also be shown by the laws of geometric optics. Figure 4(c) shows the intensity through the half-sphere as a plane-convex lens. The max intensity of light is at the point that presents the focal point of the plane-convex lens. This point is not on the surface of a sphere, as in Fig. 4(b). It is more distant because the radius of a flat surface of the plane convex lens is infinite and the optical power is smaller. The results presented here by the FDTD method are the same as predicted by laws of geometrical optics.

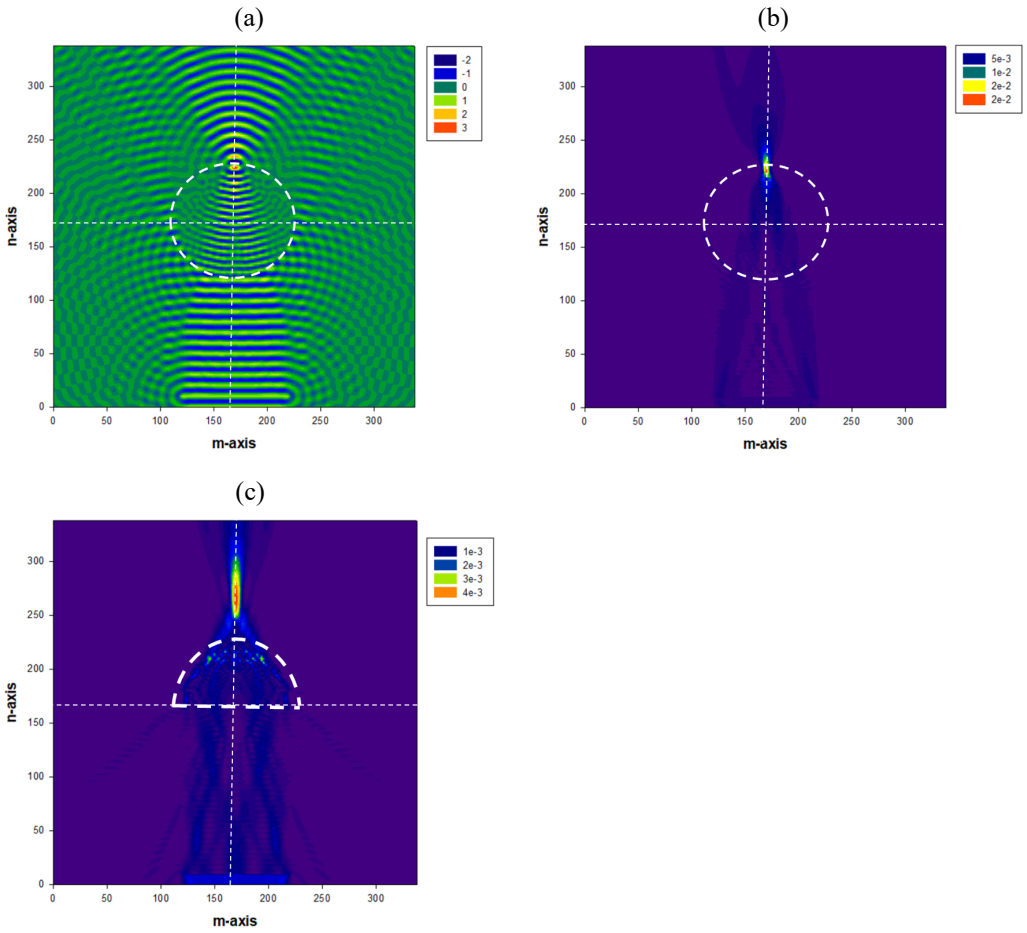

Fig. 4. Propagation of light through a spherical surface as a convex lens. (a) Electric field strength of the light that propagates through a spherical surface. (b) Intensity of the light that propagates through a spherical surface. (c) Intensity of the light that propagates through a half-sphere as a plane-convex lens.

3.3. Light propagation through the conical surface

Light propagation through the conical surface was presented in this part. The axis of the cone is set parallel to the *n*-axis, in the middle of the grid. The top of the cone is lined toward the point of the source, as in Fig. 5. Conical surface with radius $R = 50\Delta$ and height $H = 50\Delta$ was presented in Fig. 5(a) and radius $R = 50\Delta$ and height $H = 30\Delta$ was presented in Fig. 5(b). The center of the conical base is (170, 170). The relative electric constant of the medium outside of the cone is $\varepsilon_{r_2} = 2.25$ and inside the cone is $\varepsilon_{r_1} = 1$.

For the first cone total reflection is satisfied and the interior of the cone is not illuminated. Viewed from the top of the *n*-axis, the surface above the cone would be a dark area. In the case of the second cone, part of the light wave penetrates the cone

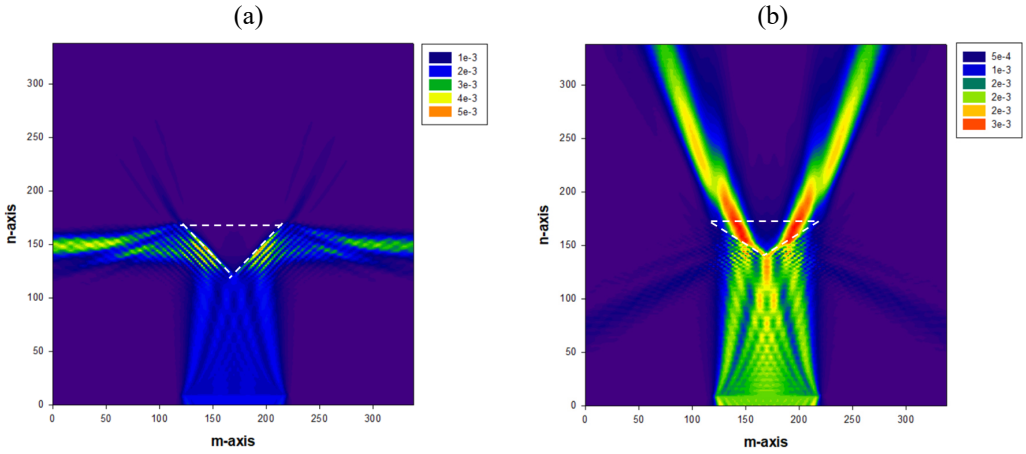

Fig. 5. The intensity of light wave propagating through the conical surface. (a) $R = 50\Delta$ and $H = 50\Delta$, and (b) $R = 50\Delta$ and $H = 30\Delta$.

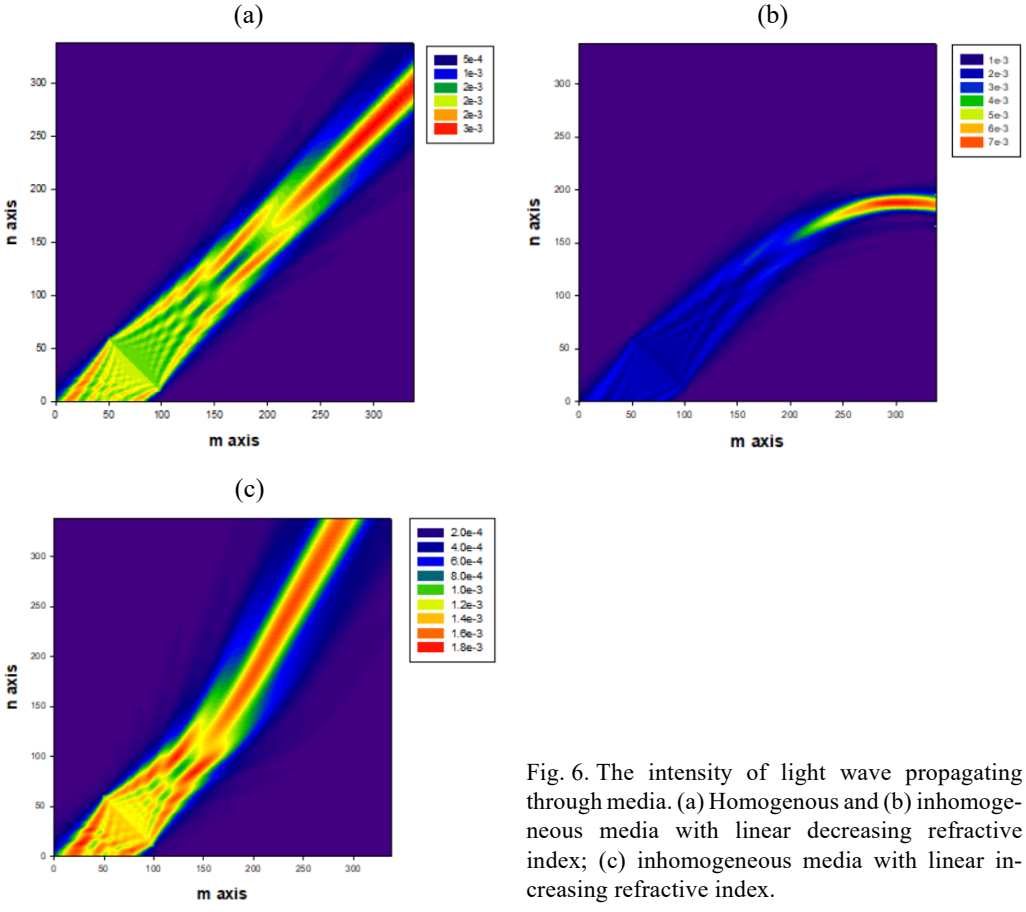

Fig. 6. The intensity of light wave propagating through media. (a) Homogenous and (b) inhomogeneous media with linear decreasing refractive index; (c) inhomogeneous media with linear increasing refractive index.

surface, and viewed from the top of the n-axis, a bright ring would be observed whose characteristics depend on the dimension conical surface.

3.4. Light propagation through inhomogeneous media

This part of the paper deals with the propagation of a light wave through an inhomogeneous media, shown in Fig. 6. The light source is linear, as in the previous cases, but at an angle of $\pi/4$ with respect to the m-axis where $n = -m + 110$. Figure 6(a) shows the propagation of light through a homogeneous medium. The direction of light propagation has not changed. Figure 6(b) shows the propagation of light through an inhomogeneous medium, where the refractive index, *i.e.*, the relative electric constant, decreases linearly as

$$\varepsilon_r(n) = \begin{cases} 2.25, & n < 100 \\ \dfrac{2.25 - 1}{100 - 200}(n - 200) + 1, & n > 100 \quad \text{and} \quad n \le 200 \\ 1, & n > 200 \end{cases} \tag{21}$$

Due to propagation through an inhomogeneous media, the beam of light bends toward media with a higher refractive index, as predicted by refraction law.

Figure 6(c) shows the propagation of light through inhomogeneous media where the relative electric constant linearly increases as

$$\varepsilon_r(n) = \begin{cases} 1, & n < 100 \\ \dfrac{1 - 2.25}{100 - 200}(n - 200) + 2.25, & n > 100 \quad \text{and} \quad n \le 200 \\ 2.25, & n > 200 \end{cases} \tag{22}$$

The bending of the light beam can be seen in Fig. 6. as predicted by refractive law.

Figure 7 shows the distribution of the intensity of light propagating through the sphere of radius $R = 50\Delta$, with relative electric constant $\varepsilon_r = 2.25$. The conductivity and magnetic constant are the same as outside of the sphere. In Fig. 7(a) intensity of visible light was presented with wavelength $\lambda = 500$ nm, while Fig. 7(b) presents the intensity of infrared light, with wavelength $\lambda = 1266$ nm. It could be seen that for shorter wavelengths the maximum of light intensity is more concentrated, while for the light of a longer wavelength, the maximum has a lower value, and is more spread out.

The influence of media conductivity on light propagation was also investigated in this paper. The distribution of light intensity that propagates in a vacuum in which the conductive sphere was located as presented in Fig. 8. The conductivity of the sphere is $\sigma = 6 \times 10^7$ S/m and the relative electric constant is $\varepsilon_r = 2.25$. The radius of the sphere is $R = 50\Delta$ and the wavelength of light is $\lambda = 500$ nm. It can be seen from the

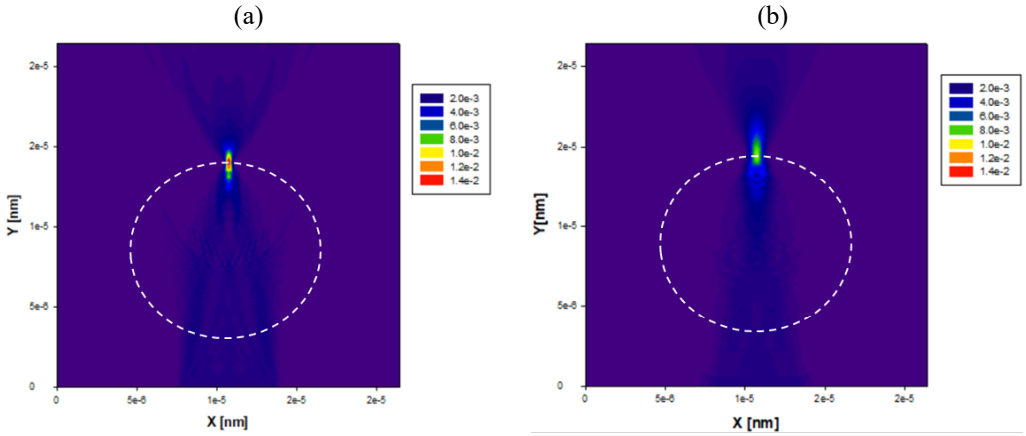

Fig. 7. The intensity of light wave through media is defined by a spherical surface with a radius $R = 50\Delta$. (a) Wavelength $\lambda = 500$ nm, visible light; (b) wavelength $\lambda = 1266$ nm, infrared light.

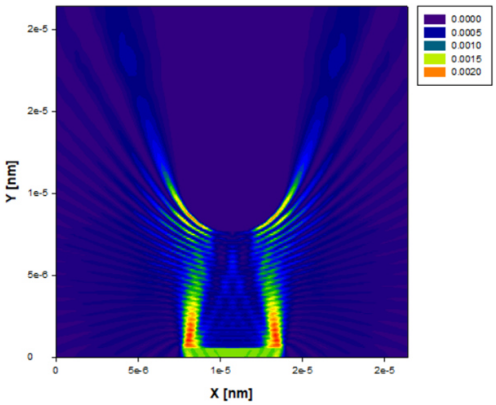

Fig. 8. Distribution of the intensity of light scattered on a conductive sphere with radius $R = 50\Delta$. The conductivity of the sphere is $\sigma = 6 \times 10^7$ S/m; the wavelength of light is $\lambda = 500$ nm.

figure that the light wave does not pass through the sphere, it is reflected from it and scattered on it, which is another indication that this model is valid.

4. Conclusion

In this work, the model for light propagation through arbitrary media was described. The model is based on Maxwell's equations in discrete form (FDTD method). In this paper light propagation was considered for several cases and the intensity of light was determined: two homogenous media bounded with plane, conical and spherical surface, inhomogeneous media. The results presented here are the same as should be obtained with laws of refraction and reflection of light.

The advantage of the model presented in this paper is that it could be applied for arbitrary inhomogeneous and conducting media. The light polarization can be arbitrarily taken and defined in the source. In this paper *s* and *p* polarization were presented. Changing of electric and magnetic field strength orientation during light propagation was taken into account. Monochromatic light was considered in this paper, but the model could be applied for other wavelengths. The model developed and presented in this paper could also be applied to polychromatic light, by simulating the propagation of light of different frequencies, *i.e.*, wavelengths and total and summing them.

The set of equations presented here was applied for linear optics, where the parameters of media are constant over time. The model could be easily modified for nonlinear optics, where the parameters of media depend on the time or they are a function of the electric and magnetic field of the propagating light. This method could be useful in spectroscopy, optical communications, optical fibers, and other fields.

Acknowledgments

The present work was supported by The Ministry of Education of the Republic of Serbia (451-03-47/ 2023-01/ 200122).

References

[1] Wang W., Zhang X., Meng Q., Zheng Y., *Propagation analysis of phase-induced amplitude apodization optics based on boundary wave diffraction theory*, Optics Express **25**(21), 2017: 25992 -26001. https://doi.org/10.1364/OE.25.025992

[2] Tseng S.H., *Modeling the sub-diffraction focusing phenomenon of light propagation through scattering medium*, Methods **136**, 2018: 75-80. https://doi.org/10.1016/j.ymeth.2017.11.001

[3] Volpe F.A., Letourneau P.-D., Zhao A., *Huygens–Fresnel wavefront tracing*, Computer Physics Communications **212**, 2017: 123-131. https://doi.org/10.1016/j.cpc.2016.10.021

[4] Makris K.G., Psaltis D., *Huygens–Fresnel diffraction and evanescent waves*, Optics Communications **284**(6), 2011: 1686-1689. https://doi.org/10.1016/j.optcom.2010.10.001

[5] Sabatyan A., Tavassoly M. T., *Determination of refractive indices of liquids by Fresnel diffraction*, Optics & Laser Technology **41**(7), 2009: 892-896. https://doi.org/10.1016/j.optlastec.2009.02.007

[6] Wang J., Zhang W., Cui Y., Teng S., *Fresnel diffraction by a square aperture with rough edge*, Optik **126**(21), 2015: 3066-3071. https://doi.org/10.1016/j.ijleo.2015.07.101

[7] Cui Y., Zhang W., Wang J., Zhang M., Teng S., *Fresnel diffraction of aperture with rough edge*, Journal of Optics **17**(6), 2015: 065607. https://doi.org/10.1088/2040-8978/17/6/065607

[8] Abedin K.M., Mujibur Rahman S.M., *Computer simulation of Fresnel diffraction from double rectangular apertures in one and two dimensions using the iterative Fresnel integrals method*, Optics & Laser Technology **44**(2), 2012: 394-402. https://doi.org/10.1016/j.optlastec.2011.08.001

[9] Abedin K.M., Mujibur Rahman S.M., *The iterative Fresnel integrals method for Fresnel diffraction from tilted rectangular apertures: Theory and simulations*, Optics & Laser Technology **44**(4), 2012: 939-947. https://doi.org/10.1016/j.optlastec.2011.11.004

[10] Abedin K.M., Islam M.R., Haider A.F.M.Y., *Computer simulation of Fresnel diffraction from rectangular apertures and obstacles using the Fresnel integrals approach*, Optics & Laser Technology **39**(2), 2007: 237-246. https://doi.org/10.1016/j.optlastec.2005.08.011

[11] Lu Z., Tan J., Qi J., Fan Z., Zhang L., *Modeling Fraunhofer diffractive characteristics for modulation transfer function analysis of tilted ring metallic mesh*, Optics Communications **284**(16-17), 2011: 3855-3861. https://doi.org/10.1016/j.optcom.2011.04.040

[12] WU Y., MA J., YANG Y., SUN P., *Improvements of measuring the width of Fraunhofer diffraction fringes using Fourier transform*, Optik **126**(23), 2015: 4142-4145. https://doi.org/10.1016/j.ijleo.2015.07.202
[13] TAN J., LU Z., LIU J., JIN P., WANG Y., *Analysis of Fraunhofer diffractive characteristics of a tilted metallic mesh for its effect on optical measurement*, Measurement Science and Technology **18**(6), 2007: 1703. https://doi.org/10.1088/0957-0233/18/6/S06
[14] ZHANG Z., BAI H., YANG G., JIANG F., REN Y., LI J., YANG K., YANG H., *Computer simulation of Fraunhofer diffraction based on MATLAB*, Optik **124**(20), 2013: 4449-4451. https://doi.org/10.1016/j.ijleo.2013.03.004
[15] BELAFHAL A., DALIL-ESSAKALI L., FAHAD M., *Fraunhofer diffraction by conical tracks*, Optics Communications **175**(1-3), 2000: 51-55. https://doi.org/10.1016/S0030-4018(99)00764-6
[16] IBNCHAIKH M., NASSIM K., BELAFHAL A., *Theoretical study of Fraunhofer diffraction by hemispherical tracks*, Phys. Chem. News **4**, 2001: 15-18.
[17] STEVANOVIC N., MARKOVIC V.M., *Diffraction pattern by rotated conical tracks in solid state nuclear track detectors*, Optics & Laser Technology **80**, 2016: 204-208. https://doi.org/10.1016/j.optlastec.2016.01.019
[18] STEVANOVIC N., MARKOVIC V.M., NIKEZIC D., *New method for determination of diffraction light pattern of the arbitrary surface*, Optics & Laser Technology **90**, 2017: 90-95. https://doi.org/10.1016/j.optlastec.2016.11.012
[19] MARKOVIC V.M., STEVANOVIC N., NIKEZIC D., *Propagation of light from dipole source and generalization of Fresnel-Kirchhoff integral*, Optik **180**, 2019: 447-454. https://doi.org/10.1016/j.ijleo.2018.11.132
[20] SHIMOBABA T., MASUDA N., ITO T., *Arbitrary shape surface Fresnel diffraction*, Optics Express **20**(8), 2012: 9335-9340. https://doi.org/10.1364/OE.20.009335
[21] SIMOVIĆ A., DRLJAČA B., SAVOVIĆ S., DJORDJEVICH A., MIN R., *Investigation of bandwidth in multimode graded-index plastic optical fibers*, Optics Express **29**(19), 2021: 29587-29594. https://doi.org/10.1364/OE.433481
[22] SIMOVIĆ A., SAVOVIĆ S., DRLJAČA B., DJORDJEVICH A., *Influence of the fiber design and launch beam on transmission characteristics of multimode glass W-type optical fibers*, Optics & Laser Technology **68**, 2015: 151-159. https://doi.org/10.1016/j.optlastec.2014.11.021
[23] DRLJAČA B., SAVOVIĆ S., DJORDJEVICH A., *Calculation of the frequency response and bandwidth in step-index plastic optical fibres using the time-dependent power flow equation*, Physica Scripta **2012**(T149), 2012: 014028. https://doi.org/10.1088/0031-8949/2012/T149/014028
[24] SULLIVAN D.M., *Electromagnetic Simulation Using Finite-Difference Time-Domain Method*, Institute of Electrical and Electronics Engineering, Inc., New York, 2020.
[25] LWIN Z.M., YOKOTA M., *Numerical analysis of SAR and temperature distribution in two dimensional human head model based on FDTD parameters and the polarization of electromagnetic wave*, AEU - International Journal of Electronics and Communications **104**, 2019: 91-98. https://doi.org/10.1016/j.aeue.2019.03.010
[26] ALISOY H.Z., BARLAZ US S., ALAGOZ B.B., *An FDTD based numerical analysis of microwave propagation properties in a skin-fat tissue layers*, Optik **124**(21), 2013: 5218-5224. https://doi.org/10.1016/j.ijleo.2013.03.085
[27] BORN M., WOLF E., *Principles of Optics*, Pergamon Press, New York, 1970.

Received December 11, 2022
in revised form May 25, 2023